Chemical Science

ROYAL SOCIETY OF CHEMISTRY

EDGE ARTICLE

View Article Online
View Journal | View Issue

Cite this: *Chem. Sci.*, 2025, **16**, 18660

All publication charges for this article have been paid for by the Royal Society of Chemistry

Received 26th June 2025
Accepted 29th August 2025

DOI: 10.1039/d5sc04734j

rsc.li/chemical-science

Engineering ultrapotent trivalent anticoagulants through hybridisation of salivary peptides from multiple haematophagous organisms

Joshua W. C. Maxwell,†[ab] Jorge Ripoll-Rozada,†[c] Angus S. Mackay,[ab] Imala Alwis,[de] Daniel J. Ford,[ab] Cameron B. J. Trought,[de] Joana A. Santos,[fg] Rhyll E. Smythe,[de] Joanna S. T. Liu,[de] Zack Zuccolotto,[de] Simone M. Schoenwaelder,[de] Shaun P. Jackson,[de] Pedro José Barbosa Pereira[fg] and Richard J. Payne *[ab]

Haematophagous organisms are a rich source of salivary anticoagulant polypeptides that exert their activity by blocking the catalytic site and one of two positively charged exosites on the host protease thrombin. Here, we describe a molecular engineering approach to hybridise post-translationally sulfated polypeptides from different blood-feeding organisms to enhance anticoagulant activity. This led to the discovery of a triply sulfated hybrid anticoagulant, XChimera, possessing fragments from flea, leech, and fly salivary polypeptides that exhibits femtomolar inhibitory activity against thrombin. The crystallographic structure of a complex of XChimera with thrombin shows that it displays a trivalent binding mode in which it simultaneously blocks three functional sites of the protease, the active site and exosites I and II. This trivalent chimera exhibited ultrapotent anticoagulant activity in a suite of *in vitro* clotting assays and was also shown to possess potent *in vivo* antithrombotic activity in a murine model of thrombosis.

Cardiovascular disease is the greatest contributor to human morbidity and mortality globally, placing health systems around the world under enormous stress.[1–3] At the core of this crisis are thrombotic disorders,[4] that are initiated by the occlusion of the vasculature by a blood clot and resultant hypoxic injury that lead to serious medical events such as stroke and myocardial infarction (heart attack).[5] The growing incidence of thrombotic events has stemmed from an ageing population and rising obesity rates, compounded by a limited number of safe and effective therapeutic options.[6] This has led to significant demand for novel therapeutics to curb the enormous burden of thrombotic disorders.[7]

Pathogenic thrombosis is caused by inappropriate activation of the 'coagulation cascade', a series of sequential proteolytic events catalysed by serine proteinases that culminates in the cleavage of fibrinogen to insoluble fibrin and simultaneous activation of platelets.[8–13] As the central enzyme of this cascade, pharmacological inhibition of the protease thrombin (FIIa) with direct thrombin inhibitors (DTIs) has become a mainstay of antithrombotic therapy in the clinic.[14,15] Despite the availability of a number of DTIs, thrombin-inhibiting anticoagulants that possess a novel mechanism of action to DTIs currently used in the clinic are still in demand,[16] particularly for use in surgical settings and the prevention of coronary artery disease.[17]

One source of powerful anticoagulants are found within the saliva of blood-feeding (haematophagous) organisms. Resulting from evolutionary pressures, haematophagous organisms have evolved a suite of salivary peptide and protein molecules to ablate thrombin-driven blood coagulation of their host, as is required for successful acquisition and digestion of a blood meal.[18] Indeed, the anticoagulant properties of leech saliva have been known for hundreds of years. The active proteinaceous anticoagulant component of this saliva, the protein hirudin, has been extensively profiled for its therapeutic qualities;[19] a recombinant form called lepirudin was used clinically for more than a decade prior to its withdrawal due to the cost of recombinant production, alongside safety concerns following anaphylactic events.[20] The impressive potency of this salivary protein stems from its highly constrained fold, mediated by a complex disulfide architecture, that orients its N-terminal

[a]*School of Chemistry, Faculty of Science, The University of Sydney, NSW, Australia. E-mail: richard.payne@sydney.edu.au*

[b]*Australian Research Council Centre of Excellence for Innovations in Peptide and Protein Science, The University of Sydney, Sydney, NSW 2006, Australia*

[c]*Instituto de Biomedicina y Biotecnología de Cantabria (IBBTEC), Consejo Superior de Investigaciones Científicas (CSIC)-Universidad de Cantabria, Santander, Spain*

[d]*Charles Perkins Centre, The University of Sydney, NSW 2006, Australia*

[e]*Heart Research Institute, Sydney, NSW 2042, Australia*

[f]*IBMC – Instituto de Biologia Molecular e Celular, Universidade do Porto, 4200-135 Porto, Portugal*

[g]*i3S - Instituto de Investigação e Inovação em Saúde, Universidade do Porto, 4200-135 Porto, Portugal*

† These authors contributed equally.

segment into the catalytic active site and its highly acidic and flexible C-terminus into exosite I.[21] Interestingly, the tyrosine residue at position 63 of hirudin was found to be post-translationally modified with an anionic sulfate group akin to the natural modifications present on human fibrinogen, an endogenous exosite-binding substrate of thrombin.[22] Exploiting post-translational tyrosine sulfation to potently inhibit thrombin through biomimicry is not unique to hirudin. Recently, we have revealed the presence of tyrosine sulfation on several other salivary anticoagulants produced by ticks,[23] mosquitoes,[24] leeches,[25] and flies.[26] In the case of the *Glossina morsitans morsitans* (tsetse) fly and many ticks, tyrosine sulfation is used to enhance binding to exosite II of thrombin as a biomimetic of the physiological thrombin substrates glycoprotein 1bα and fibrinogen-γ′ chain.[26]

In this work, we sought to exploit the diversity of potent bivalent thrombin inhibitors produced in the saliva of haematophagous organisms as scaffolds for the molecular engineering of potent chimeric anticoagulants. Specifically, we chose to target the three main regions of thrombin that mediate its haemostatic function – the active site, exosite I, and exosite II. Through this engineering approach, we arrived at a trivalent hybrid dubbed 'XChimera' which contains portions of fly, flea, and leech anticoagulants and exhibits ultrapotent inhibition of thrombin and antihaemostatic activity in a suite of *in vitro* clotting assays. This engineered peptide also exhibited superior *in vivo* antithrombotic activity compared to the gold-standard anticoagulant hirudin in a murine needle injury model of thrombosis.

Results

Engineering the exosite I-binding region of XC43

Recently, a potent thrombin-inhibiting anticoagulant was discovered in the saliva of the oriental rat flea, *Xenopsylla cheopis*, the infamous bubonic plague vector.[27] This 36-residue peptide, dubbed XC43, is a flexible substrate mimic that exhibits bivalent binding to both exosite I and the active site of thrombin, while demonstrating remarkable selectivity for this enzyme over a large number of different proteases beyond those involved in coagulation. A distinctive characteristic of this peptide, compared to other anticoagulants from blood feeders that typically possess one or more thrombin cleavage sites, is an intrinsic resistance to proteolytic cleavage by thrombin – an attractive feature for an anticoagulant in a clinical setting.[27] XC43 bears very high sequence homology within the exosite I-binding C-terminal region to the archetypal leech-derived DTI hirudin[22] and the tick-derived DTI variegin[28] (Fig. 1A). While hirudin and variegin possess a post-translationally modified sulfotyrosine (sY) residue that potentiates electrostatic interactions with the dense positive charge in thrombin's basic exosite I, XC43 has a hydrophobic valine residue (V29) in an equivalent position.

Given that post-translational tyrosine sulfation has been shown to impart an order-of-magnitude improvement in inhibitory activity for both variegin and hirudin,[22,29] we hypothesised that the potency of XC43 could be enhanced through rational engineering of synthetic variants exploiting sulfotyrosine (sY) in place of V29. First, native XC43 (**1**) was synthesised using Fmoc-strategy solid-phase peptide synthesis (SPPS) in excellent yield (12% over 73 steps, average of 97% per synthetic step) to serve as a benchmark molecule for engineered analogues (Fig. 1B and SI). Two variant forms of XC43 were subsequently designed and synthesised by SPPS to probe the importance of the valine residue, one bearing a simple V29Y replacement (**2**) and a second, post-translationally modified variant (**3**), with a V29sY replacement (Fig. 1B). When profiled in a thrombin assay using a chromogenic substrate,[23] replacing valine with tyrosine in **2** resulted in a considerable drop in potency (K_i = 502.9 pM for **2** *vs.* K_i = 28.2 pM for synthetic XC43 **1**, Fig. 1C). However, introduction of a tyrosine sulfate residue in **3** (V29sY) restored the inhibitory potency (K_i = 10 pM for **3**). The diminutive improvement in inhibitory activity of sY-containing variant **3** over native XC43 **1** was thought to be a result of unfavourable conformational changes in the vestigial C-terminal tail ($XC43_{30–36}$) induced by sY. To test this hypothesis, we next sought to hybridise the C-terminal exosite I-binding regions of variegin and hirudin into the XC43 sequence to generate more potent chimeric anticoagulants.

Towards this end, hybrid peptides were designed and synthesised that were composed of the first 28 residues of XC43 ($XC43_{(1–28)}$) and either the six exosite I-binding C-terminal residues of $variegin_{(27–32)}$ or the three C-terminal residues of $hirudin_{(63–65)}$. Chimeras were prepared with or without a tyrosine sulfate in the variable C-terminal region, giving a total of four constructs: XC43-Vari (**4**), sulfo-XC43-Vari (**5**), XC43-Hiru (**6**), and sulfo-XC43-Hiru (**7**) (Fig. 1B). Unsulfated engineered hybrid peptides XC43-Vari **4** (K_i = 83.9 pM) and XC43-Hiru **6** (K_i = 67 pM) were less potent than native XC43 **1** (K_i = 28.2 pM), whereas sulfated analogues sulfo-XC43-Vari (**5**) and sulfo-XC43-Hiru (**7**) exhibited superior activities with inhibitory constants of 6.3 pM and 5.1 pM, respectively, against α-thrombin (Fig. 1C). This represents a near 15-fold improvement in potency for **5** and **7** relative to their unsulfated counterparts, and notably corresponds to 4- and 6-fold improvements in potency compared to native XC43 (**1**), that was proposed to be due to improved interactions with exosite I. Whilst the most promising candidate **7** was less potent than the 'parent' anticoagulant hirudin, at 31 residues, sulfo-XC43-Hiru (**7**) is half the size of the full-length leech protein.

We next sought to investigate whether the improved inhibitory activity of sulfated hybrids sulfo-XC43-Vari (**5**) and sulfo-XC43-Hiru (**7**) was a result of improved exosite I-targeting of the inhibitors. To assess this, we screened anticoagulants **1–7** for their inhibitory activity against γ-thrombin (Fig. S1). Endogenously, γ-thrombin is a minor circulating form of thrombin that has a disrupted exosite I but retains the ability to activate platelets.[30] This makes γ-thrombin an excellent tool to assess the contribution of exosite I binding to the inhibition of α-thrombin. When compared to its inhibition profile against α-thrombin, native XC43 (**1**) displayed a six-orders-of-magnitude reduction in potency (K_i = 26.2 μM), suggesting that binding to exosite I is integral to α-thrombin inhibition. The remaining hybrid peptides **2–7** displayed similar reductions in inhibition profiles, with K_i values ranging from 2 to 60 μM (Fig. S1), again

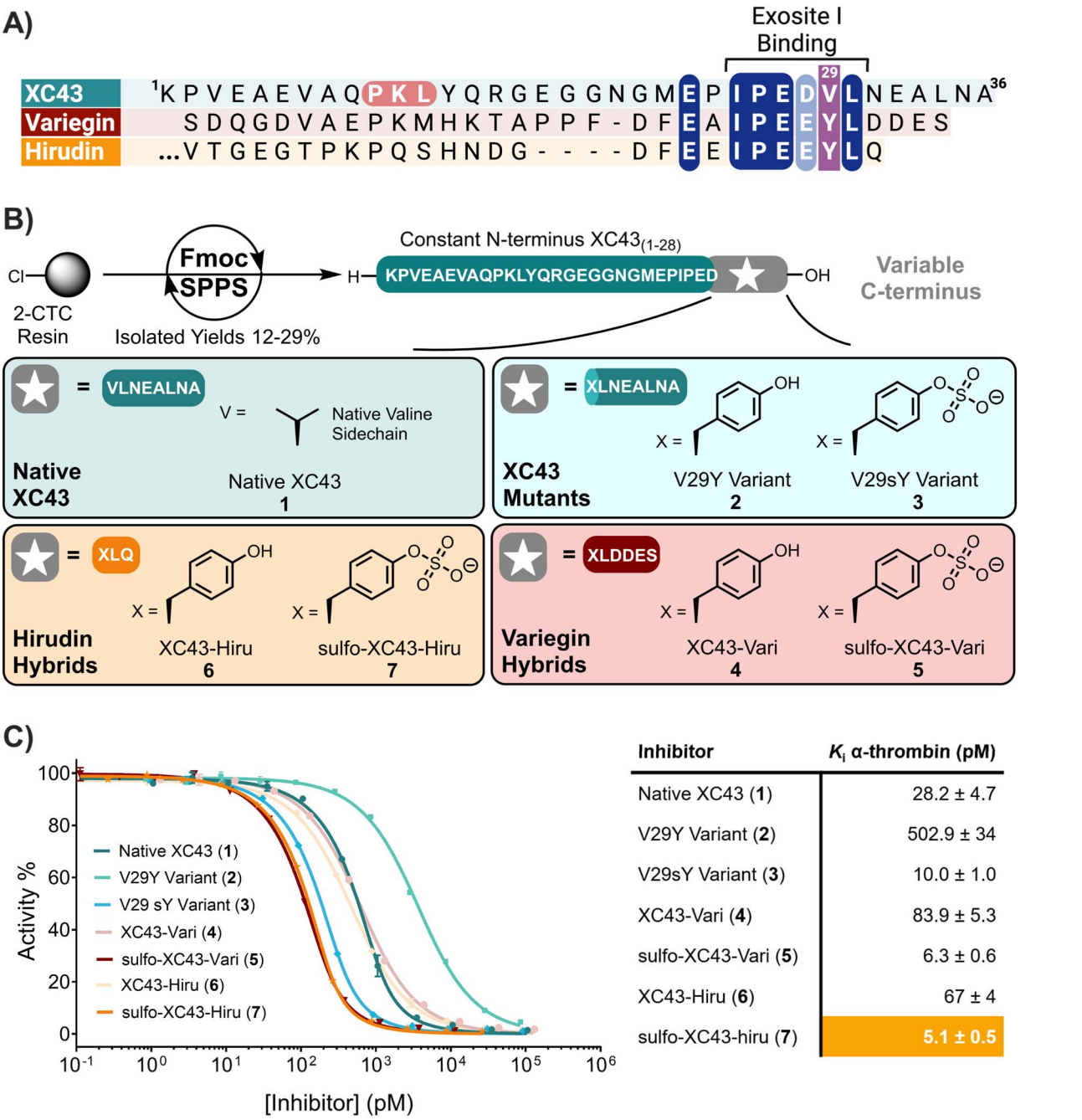

Inhibitor	K_i α-thrombin (pM)
Native XC43 (**1**)	28.2 ± 4.7
V29Y Variant (**2**)	502.9 ± 34
V29sY Variant (**3**)	10.0 ± 1.0
XC43-Vari (**4**)	83.9 ± 5.3
sulfo-XC43-Vari (**5**)	6.3 ± 0.6
XC43-Hiru (**6**)	67 ± 4
sulfo-XC43-hiru (**7**)	5.1 ± 0.5

Fig. 1 Engineering of the C-terminal region of flea thrombin inhibiting anticoagulant XC43. (A) Alignment of amino acid sequences of XC43 (UniProt entry A2IAB2), hirudin$_{(40-65)}$ (UniProt entry P09945), and variegin (UniProt entry P85800). (B) Schematic depicting the synthesis of a library of XC43 derivatives (**1–7**) using Fmoc-SPPS as outlined in the methods and SI. (C) Inhibition profiles of XC43-derived peptides (**1–7**) against α-thrombin using a chromogenic substrate assay. Data are expressed as the mean of two technical replicates and error bars plotted as SD. The inhibition constants (K_i) for the peptides (± standard errors) were determined by fitting the inhibited steady-state velocity data to the Morrison model.[31]

affirming exosite I binding as a main contributor to the observed α-thrombin inhibitory activity of these compounds.

Design and synthesis of a cleavage-resistant trivalent inhibitor of thrombin

Following initial success in engineering XC43 into a more potent sulfopeptide anticoagulant, we turned our attention to further engineering the hybrid to promote binding to exosite II. Exosite II is an additional functional region of α-thrombin and is responsible for the modulation of a myriad of procoagulant functions.[32–36] We reasoned that strong blockade of this site, in addition to the active site and exosite I, would further improve the thrombin inhibitory and anticoagulant activity of the engineered peptide. We selected the exosite II-binding region of the

tsetse thrombin inhibitor (TTI) produced in the salivary glands of the tsetse fly,[26,29,37–39] for the N-terminal elaboration of the bivalent hybrids. Specifically, we selected the most potent analogue generated above, sulfo-XC43-Hiru (**7**), as the basis of an engineered, trivalent hybrid inhibitor capable of occupying the active site, exosite I and exosite II simultaneously and, importantly, with resistance to thrombin proteolysis (Fig. 2A).

To design these trivalent hybrid inhibitors, we used the crystal structures of XC43 (PDB entry 7MJ5 [27]) and TTI (PDB entry 6TKH[26]) complexed with α-thrombin to guide the selection of an appropriate site on the N-terminal end of XC43 from which to fuse the TTI sequence. We chose to adjoin the two anticoagulant peptides between Gly21 of TTI and Ala5 of XC43, as these are in close proximity in the structures of their complexes with thrombin and are present in flexible segments of both inhibitors (Fig. S2). Following design of this hybrid anticoagulant composed of fragments of three different anticoagulants from three different species of haematophagous organisms, we set out to access the full-length 48 residue polypeptide TTI-XC43-Hiru (**8**), first in its non-sulfated form,

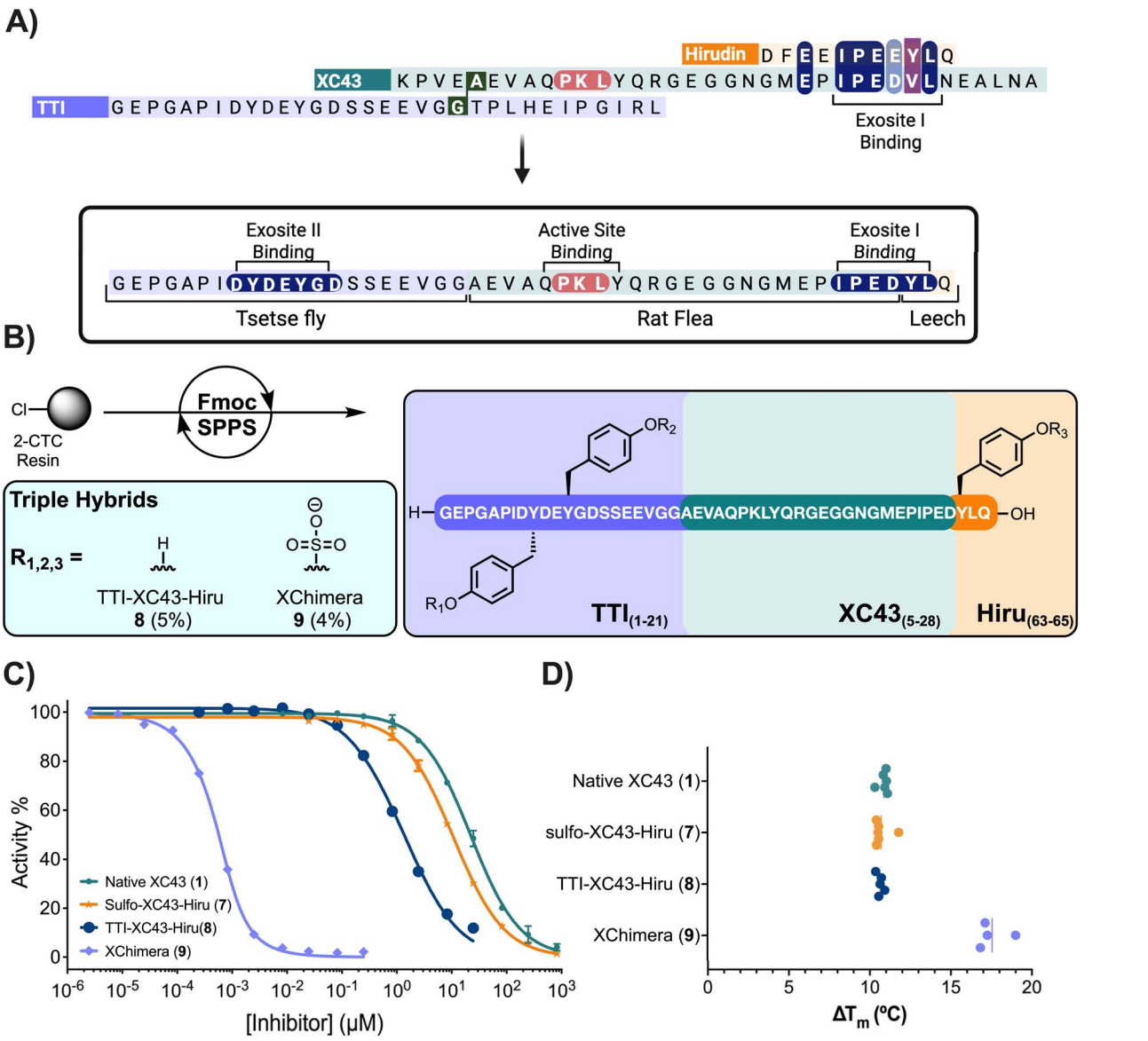

Fig. 2 Rational design, synthesis and profiling of a trivalent thrombin inhibitor. (A) Overlay of mature peptide and protein sequences of hirudin$_{(55-65)}$ (UniProt entry P09945), XC43 (UniProt entry A2IAB2) and TTI (UniProt entry O97373) and design of a chimeric inhibitor. (B) Synthesis of TTI-XC43-Hiru (**8**) and XChimera (**9**) using Fmoc-SPPS as outlined in the methods and SI (final isolated yields are provided in parentheses over all solid-phase synthesis steps). (C) Inhibition profiles of XC43-derived peptides **1**, **7**, **8** and **9** against γ-thrombin using a chromogenic substrate assay. Data are expressed as the mean of two independent experiments and error bars plotted as SD. The inhibited steady-state velocity data were fitted to the Morrison model.[31] (D) Perturbations to thermal shift of thrombin in the presence of XC43-derived inhibitors. Melting temperatures (T_m) were determined as the point of inflection in the fluorescence emission ratio of 350/330 and the difference in melting temperature (ΔT_m) was determined as the difference with thrombin alone. Data are representative of 4–6 technical replicates.

which could be generated through a single SPPS (5% overall yield over 97 synthetic steps following purification by reversed-phase HPLC; Fig. 2B). The unmodified trivalent hybrid exhibited a K_i of 1 pM against α-thrombin (*cf.* 67 pM for XC43-Hiru **6**, SI Table S1). This provided an early indication that the addition of the exosite II-binding TTI fragment improves thrombin inhibitory activity. When produced in the salivary glands of the tsetse fly, TTI has two native sites of post-translational sulfation at ^{TTI}Y9 and ^{TTI}Y12 (superscript 'TTI' designates TTI residues) that dramatically enhance its thrombin inhibitory activity.[26] Accordingly, we next set out to synthesise the triply sulfated trivalent hybrid, sulfo-TTI-XC43-sulfo-Hiru, herein referred to as XChimera (**9**), bearing two tyrosine sulfate residues in the N-terminal 21-residue TTI fragment and one in the C-terminal hirudin tripeptide fragment (Fig. 2B). Despite its length and complexity, XChimera (**9**) was produced in good yield (4% over 98 synthetic steps). XChimera (**9**) exhibited ultrapotent inhibitory activity against α-thrombin with a $K_i = 190$ fM (see Fig. S3 and Table S1). It is worth noting that this triply sulfated, trivalent inhibitor is equipotent to the clinically used form of the disulfide rich protein, hirudin, despite being a smaller, flexible, linear polypeptide. When compared to other clinically approved thrombin inhibitors, bivalirudin ($K_i = \sim$10 nM) and dabigatran ($K_i = \sim$4 nM), XChimera exhibits orders of magnitude higher potency. In addition, XChimera (**9**) exhibits increased potency compared to the naturally occurring sulfated TTI, most likely due to the addition of exosite I recognition portions from XC43 and hirudin.

We next screened the trivalent inhibitors against γ-thrombin to assess the contribution of the exosite II TTI fragment to the inhibitory activity. The unsulfated TTI-XC43-Hiru molecule lost more than five-orders of magnitude of inhibitory activity on γ-thrombin ($K_i = 360$ nM *vs.* 1 pM for α-thrombin). Strikingly, the addition of sY residues in the triply sulfated variant, XChimera, regained four-orders-of-magnitude in inhibitory activity against γ-thrombin ($K_i = 112$ pM) when compared to its unsulfated counterpart **8** (Fig. 2C). Despite these gains, the inhibitory activity against γ-thrombin is still significantly weaker than against α-thrombin, highlighting the importance of exosite I binding for potency. Nonetheless, these data show that hybrids **8** and **9** (XChimera) are *bona fide* trivalent inhibitors. Finally, we assessed the ability of XChimera to stabilise α-thrombin through a nanoDSF assay.[40] In these experiments, XChimera (**9**) provided the largest ($\Delta T_m = 17.6$ °C) stabilisation when compared to unsulfated trivalent hybrid (**8**), bivalent hybrid sulfo-XC43-Hiru (**7**), and parent inhibitor XC43 (**1**) (Fig. 2D). The addition of three tyrosine sulfate residues in XChimera (compared to trivalent hybrid **8**) was responsible for a ∼7 °C increase in the melting temperature of the complex, further highlighting the pronounced effect that addition of this 80 Da anionic PTM has on the binding to thrombin.

Structure of XChimera–human α-thrombin complex

To provide structural evidence for the ability of engineered hybrid XChimera (**9**) to occupy the active site and exosites I and II, *i.e.*, behave as a trivalent inhibitor, we sought to obtain an X-ray crystal structure of its complex with thrombin. To this end, a complex of XChimera (**9**) and α-thrombin was crystallised and its structure determined at 2.5 Å resolution. Gratifyingly, there was readily interpretable electron density for the segments of the anticoagulant contacting both exosites I and II and the active site cleft of thrombin. The crystallographic structure reveals an extended conformation for XChimera, with its N-terminal region binding to exosite II of the enzyme, before threading through the active site and onto exosite I, to which the C-terminal portion of the inhibitor binds (Fig. 3A). The exosite II-targeting region of XChimera closely resembles the parent TTI, with most interactions with thrombin being conserved. In particular, sY9 of XChimera adopts a nearly identical conformation as in native TTI, preserving the interaction with ^{T}K235 (superscript 'T' designates thrombin; Fig. 3B). Further to this, negatively charged residues ^{TTI}D8 and ^{TTI}D10 form contacts with ^{T}R233 and ^{T}R101, respectively, interactions that are conserved in XChimera. Although slightly displaced when compared to ^{TTI}sY12 and ^{TTI}E11, sY12 and E11 of XChimera still make favourable contacts with the basic ^{T}K240 and ^{T}K236 residues, respectively, of the protease (Fig. 3B). As in the crystal structure of TTI[26] for the region between the active site and exosite II, XChimera$_{(13-21)}$ is disordered in the crystal structure with thrombin, suggesting conformational flexibility in this segment of the inhibitor. In contrast, the active site binding region of XChimera binds in a substrate-like manner to the enzyme. As with native XC43, the crystal structure shows the amide bond between K28 and L29 of XChimera intact and making identical contacts to those observed in the parent peptide (Fig. 3D). In contrast to the active site binding residues, there is considerable structural dissonance between XC43 and the engineered C-terminal tail of XChimera at exosite I. Indeed, the anionic *O*-sulfate group of residue 46 of XChimera (derived from hirudin) forms a salt bridge (3.4 Å) with the cationic ε-amine of ^{T}K81 (Fig. 3C). By contrast, native XC43 does not make any contacts with ^{T}K81, suggesting that this salt bridge may contribute to the improved inhibitory activity observed following hybridisation of XC43 with hirudin. Furthermore, the analogous ^{H}sY63 in sulfo-hirudin (superscript 'H' denotes hirudin) also forms a salt bridge with ^{T}K81, an interaction known to confer an order-of-magnitude improvement in potency in the full-length hirudin protein.[22] Replacement of the C-terminal residues of XC43 with the hirudin-derived C-terminus causes a conformational rearrangement of this region and its preceding segment, when comparing XChimera to native XC43 (Fig. 3E). Remarkably, the last six residues of XChimera, from P43 to Q48, adopt an overall conformation, including an α-helical turn, that is nearly identical to that of native hirudin, despite containing only three residues derived from that protein. When superposed onto the experimental models of native TTI, XC43, and hirudin, as determined in complex with α-thrombin, XChimera (**9**) exhibits near-perfect structural homology to its three parent anticoagulants at exosite I, exosite II, and the active site. Beyond affirmation of the molecular engineering approach applied in this work, we reasoned that the evidence for the trivalent blockade of thrombin found in this co-crystal structure may make

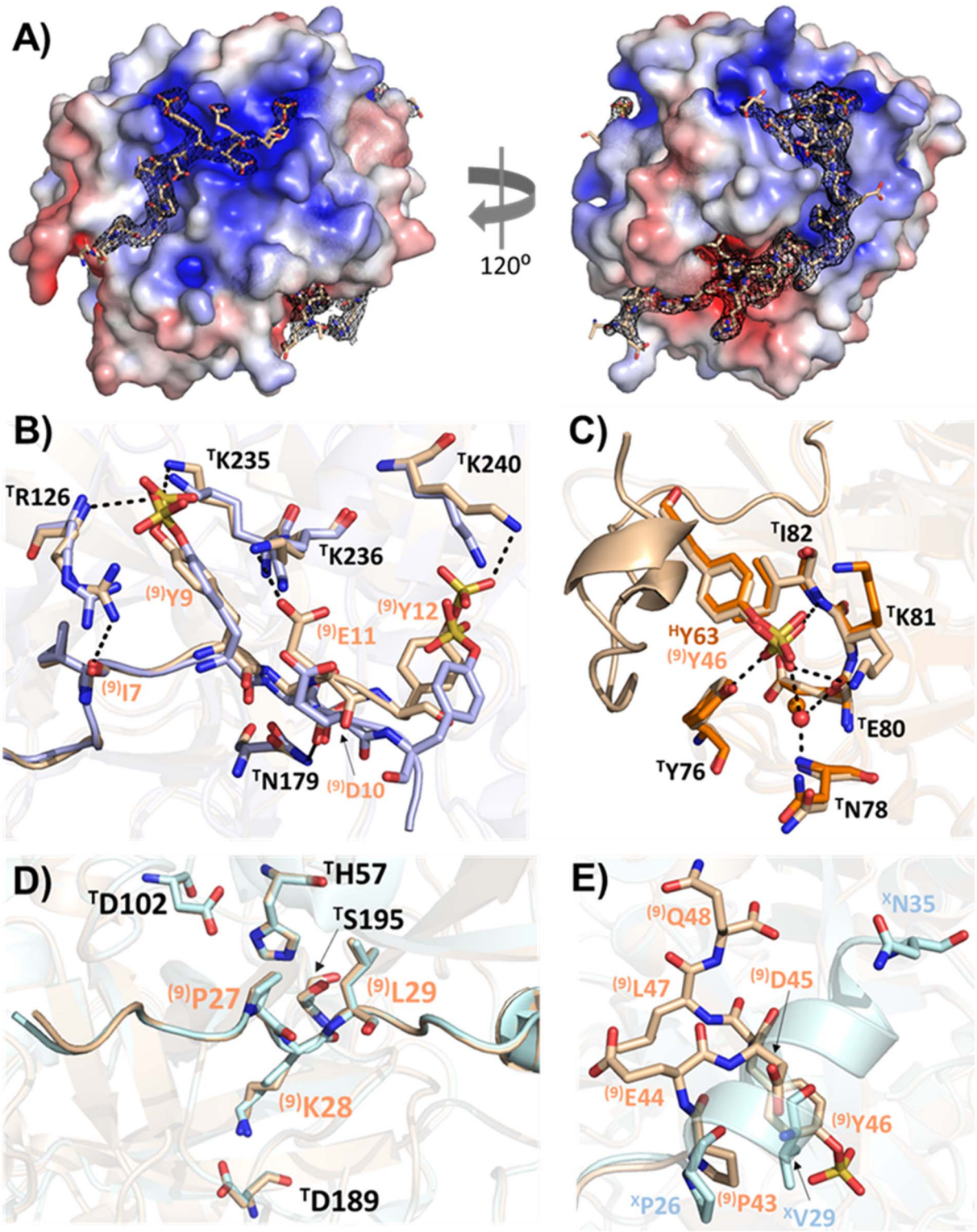

Fig. 3 XChimera (**9**) is a trivalent binder of human α-thrombin. (A) The acidic N-terminal segment (residues 1–12) of XChimera (**9**) (stick model with nitrogen atoms blue, oxygen red, sulfur yellow, and carbon tan; PDB entry 8RTN) binds to the exosite II (left) of thrombin (solid surface representation with mapped surface electrostatic potential [blue, positive; red, negative]), whereas the C-terminal segment (residues 22–48) occupies the active-site cleft and recognises the exosite I of the proteinase (right). The 2Fo–Fc electron density map (contoured at 0.9σ) for XChimera (**9**) is displayed as a black mesh. Thrombin orientations in the left and right panels are related through a 120° rotation around *y*. (B) Main interactions between the sulfotyrosine-containing motif (residues 7–12) of XChimera (**9**) (coloured as in (A)) and the exosite II of thrombin (transparent tan cartoon with selected residues as sticks, colour-coded as for XChimera (**9**)). The structural superposition of human α-thrombin in complex with TTI (mauve; PDB entry 6TKG) is represented as for the XChimera (**9**) complex. (C) Close-up view of the interactions between the

XChimera (**9**) a promising therapeutic anticoagulant candidate with an unprecedented thrombin inhibitory mechanism for further investigation.

Evaluation of the antithrombotic potential of XChimera *in vitro* and *in vivo*

To be a useful therapeutic, peptidic anticoagulants must be able to resist the proteolytic activities of plasma enzymes; rapid cleavage leads to intractable pharmacokinetic profiles for many peptide drug candidates.[41] We investigated the stability of XChimera (**9**) in pooled human plasma, alongside precursor peptides native XC43 (**1**) and sulfo-XC43-Hiru (**7**). Both native XC43 (**1**) and sulfo-XC43-Hiru (**7**) underwent rapid amidolysis between P2 and V3 following incubation with plasma, but the resultant cleavage product remained stable to 24 hours (Fig. S4). Pleasingly, XChimera (**9**) remained intact for 24 hours, demonstrating remarkable stability for a non-disulfide constrained linear peptide (Fig. 4C). We hypothesise the long plasma stability of XChimera (**9**) stems from it being comprised of the major anticoagulant molecules from blood-feeding organisms. The rapid inactivation of these anticoagulant peptides in host plasma would result in a greatly decreased ability to acquire a blood meal, placing an evolutionary pressure for these peptides to be proteolytically stable to plasma proteases. We also confirmed that XChimera (**9**) retained resistance to thrombin proteolysis, with <10% cleavage observed after incubation with α-thrombin for 4 h at 37 °C (Fig. 4D and S5). Finally, the selectivity of XChimera (**9**) for thrombin over other structurally related proteases in the coagulation cascade (*e.g.*, FXa, FXIa, αFXIIa, and plasma kallikrein) was assessed, as selectivity for a single haemostatic protease can be challenging to achieve for anticoagulants (Fig. S6). Pleasingly, XChimera (**9**) selectively inhibited α-thrombin without blocking these other proteases and, as such, downstream anticoagulant effects (*in vitro* and *in vivo*) can be attributed to the blockade of thrombin activity.

Having confirmed that XChimera (**9**) is stable in plasma and exhibits ultrapotent and selective inhibition of α-thrombin, mediated by interactions with both exosites and the active site, we next moved to assess the potential of the trivalent inhibitor as an anticoagulant agent. To this end, we first assessed whether XChimera could prolong the *in vitro* activated partial thromboplastin time (aPTT) of pooled human plasma. When compared head-to-head with precursor inhibitors XC43 (**1**) and sulfo-XC43-Hiru (**7**), trivalent hybrid XChimera (**9**) demonstrated the most potent anticoagulant activity (Fig. 4A). We next assessed the ability of XChimera (**9**) to modulate the generation of thrombin using pooled human plasma in a calibrated automated thrombogram experiment. While both XC43 (**1**) and sulfo-XC43-Hiru (**7**) were able to induce a dose-dependent lag effect in the generation of thrombin following initiation with tissue factor, XChimera (**9**) led to the most pronounced modulation of thrombin generation and delay in the production of thrombin in a dose dependent manner (Fig. 4B and S7). It is known that thrombin generation is highly sensitive to modulation of the exosites of thrombin. As such, the blockage of both exosites by XChimera (**9**) may be responsible for its improved potency.

Given the crucial role of platelets in potentiating thrombosis, we next sought to examine the ability of the trivalent hybrid XChimera to inhibit *ex vivo* platelet activation initiated by thrombin. In these experiments, XChimera (**9**) was added to washed platelets and then α-thrombin (0.5 nM) used to initiate platelet aggregation. XChimera (**9**) exhibited a potent antiplatelet effect, significantly disrupting platelet aggregation even at very low concentrations (IC_{50} < 400 pM, Fig. 4E). Recently, γ-thrombin has been shown to activate platelets by interacting with PAR-4 through its available exosite II.[30,42,43] To probe whether XChimera (**9**) could block this alternative platelet aggregation pathway, we measured its antiplatelet effect against γ-thrombin-initiated aggregation. Interestingly, XChimera (**9**) was also capable of potently inhibiting this pathway of platelet aggregation (IC_{50} ~8000 pM), whereas bivalent inhibitor sulfo-XC43-Hiru (**7**), notably missing an exosite II-binding region, was not capable of inhibiting aggregation in response to 20 nM γ-thrombin (Fig. 4E). These data highlight the need for the exosite II binding region in XChimera for blockade of γ-thrombin-initiated platelet aggregation, *cf.* active site and exosite I binding by sulfo-XC43-Hiru (**7**) that inhibited α-thrombin-initiated platelet aggregation.

Finally, we sought to compare the anticoagulant activities of XChimera (**9**), together with the most potent bivalent inhibitor sulfo-XC43-Hiru (**7**), *in vivo*. In initial studies we assessed the ability of sulfo-XC43-Hiru (**7**) and XChimera (**9**) to prolong the *ex vivo* aPTT following intravenous administration to mice, an organism where thrombin has a highly conserved role and structure (>80% amino acid sequence identity) to the human protein, particularly in the regions targeted by XChimera (**9**), *i.e.* the active site and exosites I and II. When administered at 1 mg kg^{-1}, sulfo-XC43-Hiru (**7**) was able to prolong the aPTT of mice between 2- and 3-fold of baseline levels for an hour following bolus injection. Interestingly, when XChimera (**9**) was

sulfated Y46 of XChimera (**9**) and the exosite I of the proteinase (selected residues are represented and coloured as in (B)). Superposed human α-thrombin in complex with hirudin (orange; PDB entry 2PW8) is shown with selected residues of the proteinase represented as for the XChimera (**9**) complex. For clarity, only Y63 of hirudin is shown. Water molecules involved in the recognition of sulfate groups of Y46 (XChimera (**9**)) or Y63 (hirudin) are represented as red and orange spheres, respectively. (D) Close-up on the active site of the superposed α-thrombin molecules complexed to either XChimera (**9**) or XC43 (pale cyan; PDB entry 7MJ5). Residues at positions P2, P1, and P1′ from both inhibitors (in XChimera P27, K28, and L29, respectively) are represented as sticks and colour-coded as in (B). The catalytic triad (H57, D102 and S195) and D189 at the bottom of the S1 specificity pocket of the proteinase are represented as sticks and colour-coded as for the inhibitors. (E) Structural differences between XC43 and XChimera (**9**) (represented as in (D)) at the exosite I due to the substitution of the XC43 C-terminal region (residues V29-A36) by the C-terminal and tyrosine-sulfated region of hirudin (Y63-Q65). Dotted black lines represent hydrogen bonds and superscripts ^{T}, ^{H}, ^{X}, and $^{(9)}$ denote residues corresponding to α-thrombin, hirudin, XC43, and XChimera (**9**) molecules, respectively.

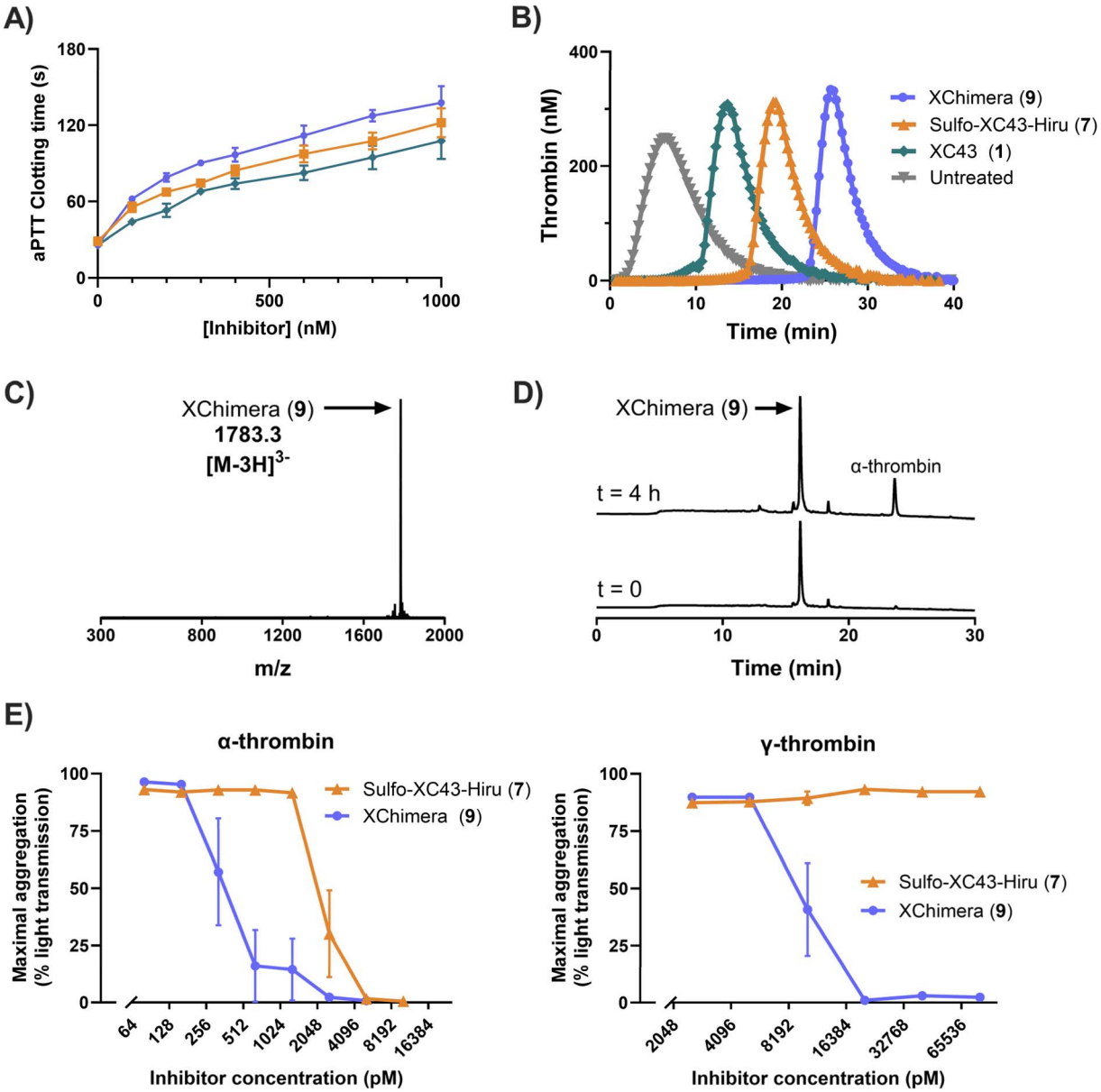

Fig. 4 *In vitro* assessment of the anticoagulant potential of thrombin inhibitors **1**, **7** and **9**. (A) Effect of the thrombin inhibitors on the aPTT of human plasma *in vitro*. See (B) for key. (B) Calibrated automated thrombogram of human plasma in the presence of 120 nM **1**, **7** and **9**. (C) ESI mass spectrum of XChimera (**9**) following incubation in pooled human plasma for 24 hours at 200 μM. Data are presented as the average mass spectrum over the total ion current. (D) Analytical HPLC chromatograms ($\lambda = 214$ nm) of XChimera (**9**) prior to ($t = 0$) and following incubation with human α-thrombin for 4 h at 37 °C. (E) Examination of the activity of XChimera (**9**) on α- and γ-thrombin-induced platelet aggregation. Washed human platelets isolated as described in the methods section were preincubated with vehicle, or the indicated concentration of XChimera (**9**) or sulfo-XC43-Hiru (**7**), prior to addition of α- or γ-thrombin (0.5 or 20 nM, respectively). Platelet aggregation was analysed as described in the methods section. Data are represented as the mean ± SEM of % maximal platelet aggregation in response to α- (left) and γ-thrombin (right) resulting from experiments performed with at least four independent blood donors ($n = 4$–6).

administered at the same dose the aPTT was prolonged to between 4- and 5-fold of baseline levels, outside the ideal therapeutic window for an anticoagulant (Fig. 5A). However, bolus administration of XChimera (**9**) at a lower dose of 0.5 mg kg^{-1} provided steady prolongation of aPTT between 2- and 3-fold of baseline for 60 minutes (Fig. 5A). Based on these data, we moved forward with XChimera (**9**) as a lead candidate to assess *in vivo* anti-thrombotic activity in a murine needle injury model of thrombosis. In this model, thrombus volume and fibrin deposition were assessed post-injury.[24] Given the potency of XChimera (**9**), we wanted to compare its efficacy to the clinical anticoagulant, hirudin, administered at 1 mg kg^{-1}. Pleasingly, although administered at a lower dose (0.5 mg kg^{-1}), XChimera (**9**) was able to limit overall fibrin deposition and thrombus volume at the site of injury in a comparable manner to hirudin (Fig. 5B–F).

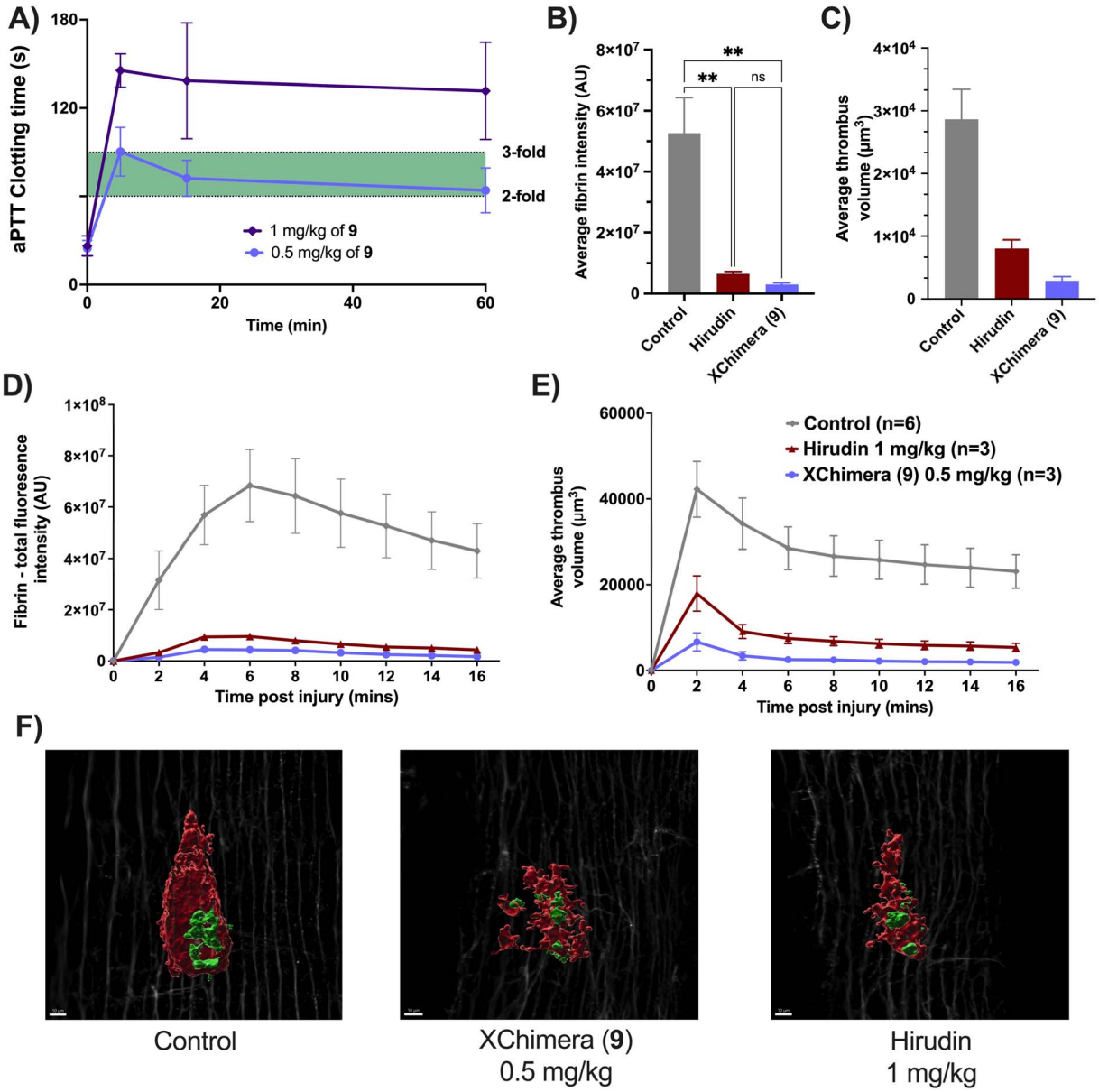

Fig. 5 *In vivo* evaluation of XChimera (**9**) in a murine model of thrombosis. (A) *Ex vivo* aPTT measurements following bolus intravenous administration of XChimera (**9**) at varying doses. (B) Average fibrin intensity over duration of measurement. (C) Average thrombus volume over duration of measurement. (D) Time course of fibrin intensity following injury with and without treatment. (E) Time course of thrombus volume following injury with and without treatment. (F) Exemplar images of thrombus following needle injury after treatment with **9** or hirudin. Images were acquired 15 min post injury. Fibrin is represented in green and platelets in red.

Conclusions

Despite the global burden of cardiovascular diseases, current treatment options remain largely inadequate. Modern anticoagulants developed for thrombotic events associated with cardiovascular diseases are required to modulate the complex interplay between the elements of the haemostatic system. In the context of myocardial infarction, patients who undergo primary percutaneous coronary intervention (PCI) require the administration of antithrombotic drugs to prevent re-thrombosis or inhibit in-stent thrombosis. One leading treatment option involves bolus infusion of the hirudin-inspired, bivalent DTI bivalirudin, which has been shown to improve overall survival rates when compared to PCI alone.[44] However, despite being efficacious in this setting, bivalirudin has significant limitations due to its short plasma half-life (~30 min) *in vivo*, which limits its application in other thromboembolic disorders. As an ultrapotent, cleavage-resistant thrombin inhibitor that uniquely occupies three distinct binding sites of thrombin (the active site, exosite I and exosite II) we anticipate that XChimera (**9**) may have the potential to address the limitations of currently employed anticoagulants. Moreover, the molecular engineering strategy employed in this work, whereby multiple peptide ligands can be hybridised to optimise potency

and stability, may be useful in the design of future anticoagulants and other therapeutic candidates where disruption of multiple protein–protein interaction sites within a given protein target is desired.

Methods

Ethics

All procedures involving the collection of blood from healthy human donors were approved by the University of Sydney Human Research Ethics Committee (HREC, Project 2014/HE00024 2014/244) and all studies conformed to the principles outlined in the Declaration of Helsinki. Written informed consent was obtained from all human research participants. All procedures involving the use of animals were performed as approved by the University of Sydney Animal Ethics Committee (protocol 2021/1912).

SPPS materials

Peptide synthesis reactions were performed using DMF purchased from Labscan. DMF used in wash steps was purchased from Ajax. Coupling reagents, Fmoc-protected amino acids and resins used for SPPS were purchased from Bachem, Novabiochem, GL Biochem or AK Scientific. Any manual SPPS steps were undertaken in polypropylene syringes bearing Teflon filters (Torviq).

General solid-phase peptide synthesis conditions

Synthesis was undertaken using a Biotage Syro I parallel peptide synthesiser. Preloaded resin in polypropylene reaction vessels was treated with 40% (vol/vol) piperidine in DMF (800 μL) for 4 min with intermittent shaking, drained by vacuum *in situ*, followed by treatment with 20% (vol/vol) piperidine in DMF (800 μL) for 4 min with intermittent shaking, drained, and washed with DMF (4 × 1.2 mL) with intermittent shaking. For canonical amino acids, the resin was then treated with a solution of the required Fmoc-X_{aa}-OH (4 eq.) and Oxyma® (4.4 eq.) in DMF (400 μL), then 1% (wt/vol) solution of 1,3-diisopropyl-2-thiourea in DMF (400 μL) and a solution of *N*,*N*′-diisopropylcarbodiimide (4 eq.) in DMF (400 μL) was added. Couplings were performed at 40 °C for 30 min using a heating block and shaken intermittently. The resin vessel was then drained as before and washed with DMF (4 × 1.2 mL). Unreacted amine groups were then acetylated by treatment with 5% (vol/vol) Ac_2O and 10% (vol/vol) i-Pr_2NEt in DMF (800 μL) for 6 min at room temperature and shaken intermittently. Resin vessels were drained and washed with DMF (4 × 1.2 mL). These steps were repeated as necessary for the synthesis of a desired peptide sequence.

Modified coupling cycle for Fmoc-Tyr(OSO_3nP)-OH

Fmoc deprotection was performed as described above. A solution of Fmoc-Tyr(OSO_3nP)-OH[45] (2 eq.) and Oxyma® (2.2 eq.) in DMF (400 μL) was then added to the reaction vessel containing the resin, followed by the addition of a solution of 1% (wt/vol) 1,3-diisopropyl-2-thiourea dissolved in DMF (400 μL) and lastly a solution of *N*,*N*′-diisopropylcarbodiimide (2 eq.) in DMF (400 μL). This coupling was performed at an elevated temperature using a heating block at 40 °C for 90 min and intermittent shaking. The vessel was vacuum drained and washed with DMF (4 × 1.2 mL), as above. The resin was then capped and washed as above.

Preparative cleavage from resin

Resin (25 μmol) was washed with CH_2Cl_2 (10 × 5 mL) and filtered *in vacuo*. Then, a mixture of TFA/TIS/H_2O (8 mL, 90 : 5 : 5, v/v/v) was prepared before the addition of solid NH_4I (10 eq., 36 mg, 250 μmol). This cleavage cocktail was then briefly sonicated to facilitate as much dissolution of ammonium iodide as possible before being added to the resin and shaken for 2 h at room temperature. The filtrate of this cleavage was collected, and the solution was concentrated under a stream of nitrogen. The crude peptide was precipitated by adding diethyl ether (50 mL) and centrifuged (6 min at 6000 *g*). The supernatant was carefully decanted to obtain the crude peptide as a pellet.

Neopentyl sulfate ester deprotection

Neopentyl-protected crude peptide (25 μmol) was dissolved in a buffer composed of 6 M Gnd·HCl and 200 mM Na_2HPO_4 and the pH adjusted to ∼8 with 5 M NaOH. The reaction mixture was then heated to 37 °C until complete conversion to the native tyrosine sulfate ester was observed by UPLC-MS analysis (16–48 h).

Characterisation data for peptides/sulfopeptides **1–9** can be found in the SI (Fig. S8–S16).

Thrombin inhibition assay

The inhibition of the amidolytic activity of human α- and γ-thrombin (Prolytix) was followed spectrophotometrically using Tos-Gly-Pro-Arg-pNA (Chromozym TH, Roche) as chromogenic substrate. The assays were performed in 50 mM Tris–HCl pH 8.0, 50 mM NaCl, 1 mg per mL bovine serum albumin with 0.2 nM human α- or γ-thrombin, 100 μM substrate, and varying concentrations of a given inhibitor. The concentration of each inhibitor variant was determined using an infrared spectrometer (Direct Detect, Millipore). All reactions were initiated by the addition of thrombin and carried out at 37 °C in 96-well flat-bottom microtiter plates. Reaction progress was monitored at 405 nm for 60 min, with measurements taken every 5 min on a multi-mode microplate reader (Synergy 2, BioTek). All measurements were performed in duplicate. Inhibition constants (K_i) were determined according to a tight-binding inhibitor model, using the Morrison equation[31] with Prism 9 (GraphPad Software), and are summarised in Table S1.

Complex preparation and crystallisation of α-thrombin : XChimera (9) complex

Human α-thrombin (Prolytix) in 50% (vol/vol) glycerol/water was prepared at 8.4 g L^{-1} in 20 mM HEPES pH 7.5, 125 mM NaCl by ultrafiltration using a 2 kDa cutoff centrifugal device (Sartorius). A 4.5-fold molar excess of the inhibitor in the same buffer was mixed with the protease and incubated on ice for 45

minutes. The resulting complex at 6.6 g L^{-1} was screened with different commercial crystallisation kits at 20 °C using the vapor diffusion sitting-drop method and an Oryx4 LCP crystallisation robot (Douglas Instruments). Single crystals belonging to the H32 space group were obtained after 5–7 days from drops consisting of equal volumes (0.5 μL) of protein complex and precipitant solution (0.2 M lithium citrate tribasic tetrahydrate and 20% (wt/vol) PEG 3350) equilibrated against 100 μL of reservoir solution.

Data collection and processing

Prior to data collection, the crystals were cryoprotected by brief immersion in mother liquor supplemented with increasing concentrations [5, 10 and 15% (vol/vol)] of glycerol and flash-cooled in liquid nitrogen. X-ray diffraction data were collected from a single cooled (100 K) crystal (3600 images in 0.1° oscillation steps and 0.05 s exposure), recorded on a PILATUS3 X 6M (DECTRIS) detector using a wavelength of 0.9793 Å at beamline BL13-XALOC[46] of the ALBA Synchrotron (Cerdanyola del Vallès, Spain). Data were integrated with XDS[47] and reduced with utilities from the CCP4 program suite.[48] Data collection statistics are summarised in Table S2. The diffraction dataset (doi: **https://doi.org/10.15785/SBGRID/1078**) was deposited with the SBGrid Data Bank (**https://data.sbgrid.org/**).[49]

Structure determination and refinement

The structure of the complex was solved by molecular replacement with Phaser[50] using the coordinates of free wild-type human α-thrombin (PDB entry 3U69).[51] Alternating cycles of model building with Coot[52] and refinement with the PHENIX suite[53] were performed until model completion (refinement statistics are summarised in Table S2). All crystallographic software was supported by SBGrid.[54] Refined coordinates and structure factors were deposited at the Protein Data Bank with accession number 8RTN (**https://doi.org/10.2210/pdb8RTN/pdb**).

aPTT assay

Anticoagulants were characterised *in vitro* using the activated Partial Thromboplastin time (aPTT).[55] Measurements using human plasma were performed on a BFT II Analyzer (Siemens Healthineers) according to the manufacturer's instructions, as we have described previously.[45] Where plasma volumes were limited (*ex vivo* mouse plasma samples), aPTT was assessed in Nunc 384-well polystyrene plates (Cat. No. Z723010, Sigma-Aldrich) *via* changes in plasma opacity at 405 nm using a ClarioSTAR plate reader (BMG Labtech) fitted with dual injectors heated to 37 °C. Analysis was performed using BMG Labtech analysis software (MARS). Dade Actin™ FS Activated PTT Reagent (Cat. No. 10445710) and calcium chloride 0.025 M solution (Cat. No. 10446232) were both sourced from Siemens Healthcare, Australia. Lyophilised pooled human reference plasma (Pooled Norm, Cat. No. 00539) was purchased from Diagnostica Stago, Australia and New Zealand. Pooled human plasma was reconstituted as per manufacturer's instructions. Pooled platelet-poor plasma was pooled from 3–5 C57BL/6 mice, following collection into 3.8% (wt/vol) sodium citrate.

Calibrated automated thrombinoscope (CAT)

Thrombin generation was measured using a Hemker Calibrated Automated Thrombinoscope (Diagnostica Stago) using a Fluoroskan Ascent® plate reader (Thermo Scientific, MA, United States), according to manufacturer's instructions (Diagnostica Stago – previously "Thrombinoscope BV", Maastricht, The Netherlands).[38,56] Normal lyophilised human pooled plasma (Pool Norm #00539, Diagnostica Stago S.A.S., Asnières-sur-Seine, France) was reconstituted and incubated for 30 min at 37 °C. Vehicle and various inhibitor concentrations were incubated in plasma post 30 min incubation. All experiments were conducted in triplicate in 96-well microplates for fluorescence-based assays (M33089, Thermo Scientific, MA, United States) and calibrated using untreated plasma and a thrombin calibrator (#86192, Diagnostica Stago S.A.S., Asnières-sur-Seine, France).

Plasma stability assay

The peptides (10 mM stock in DMSO) were added to citrated human plasma (Sigma-Aldrich) to a concentration of 200 μM. The peptides were incubated at 37 °C for 24 h before being quenched with three volumes of 1 : 1 (vol/vol) MeOH : MeCN. The samples were centrifuged at 13 500 rpm for 5 min before removing an aliquot of the supernatant (20 μL) that was diluted with water (20 μL) and analysed by reversed-phase UPLC-MS.

Thrombin cleavage assay

To detect enzymatic cleavage by α-thrombin, XChimera (25 μM) was incubated for 4 h with human α-thrombin (1 μM, Prolytix ref. HCT-0020) in 25 mM Tris–HCl pH 8.0, 150 mM NaCl at 37 °C. The reaction was quenched by the addition of 0.1% (vol/vol) formic acid in H_2O. A Waters Alliance e2690 HPLC system operating with a 2998 PDA detector (λ = 210–400 nm), an Alliance series column heater at 40 °C, and a Waters XBridge C18 column (5 μm, 4.6 × 250 mm) were used to acquire analytical HPLC chromatograms of XChimera prior to the addition of thrombin (t = 0), and XChimera and its cleavage products following incubation (t = 4 h). Analytical HPLC was performed at a flow rate of 1 mL min^{-1} using mobile phases consisting of 0.1% (vol/vol) TFA in H_2O (Solvent A) and 0.1% (vol/vol) TFA in MeCN (Solvent B) over a linear gradient of 1–60% B over 30 min. The extent of cleavage was calculated based on the relative integrals of the parent peptide and its cleavage products, as determined by analytical HPLC (λ = 214 nm).

Platelet aggregation studies

Washed platelets, prepared as described previously,[57] were stimulated with α- or γ-thrombin (0.5 and 20 nM, respectively), in the presence of calcium (1 mM) and fibrinogen (500 μg mL^{-1}). All aggregations were initiated by stirring platelet suspensions at 800 rpm for 10 min at 37 °C in a four-channel automated platelet analyser (AggRAM, Helena Laboratories). The extent of platelet aggregation was defined as the percentage (%) change in optical density as measured by the automated platelet analyser and expressed as % maximal aggregation.

Anaesthesia and surgical setup

Unless otherwise indicated, all mouse experiments were performed under similar conditions. Mice were anaesthetised with 5% (vol/vol) isoflurane for initial induction (3–5 min in induction chamber) and then maintained with 2–3% (vol/vol) isoflurane, with constant 1 L min^{-1} oxygen supplementation. Anaesthesia was confirmed with a negative pedal reflex before surgery and checked regularly during all procedures. In other experiments indicated, mice were anaesthetised with a mixture of ketamine (125 mg kg^{-1}) and xylazine (12.5 mg kg^{-1}), injected intraperitoneally. Mice were temperature maintained at 37 °C using a rectal temperature probe, with a veterinary-grade heat mat and an overhead infrared heat lamp.

Drug delivery was achieved intravenously, through the jugular vein. A small opening was made in the jugular vein to allow for insertion of a catheter made of silicone tubing. This catheter was connected to a 1 mL syringe containing the inhibitor of interest for delivery at the appropriate concentration. This syringe was connected to an infusion pump which delivered a 50 μL bolus, with or without subsequent infusion, at a constant defined rate.

Mouse plasma collection

Mouse plasma was collected from adult C57BL/6 mice for *in vitro* aPTT experiments. Mice were anaesthetised as above, and whole blood collected from the inferior vena cava using a 29 G needle into a syringe containing 3.8% (wt/vol) sodium citrate. Blood samples were centrifuged at 5000 rpm for 15 min at 4 °C to retrieve platelet-poor plasma. Plasma samples were then stored at −30 °C until use in *in vitro* aPTT assays. Plasma was kept frozen no longer than 3 months.

Needle injury model

Recombinant hirudin (160 000 ATU, Lot No. FB1756) was purchased from Hyphen-Biomed (France) and prepared in 1 mL distilled water at a concentration of 17.75 mg mL^{-1}. Synthetic XChimera (**9**) was prepared in 1× Tyrodes buffer (pH 7.4) at a concentration of 5 mg mL^{-1}. Ketamine (150 mg kg^{-1}) and xylazine (15 mg kg^{-1})-anesthetised, oxygen-supplemented C57BL/6J male mice (15–25 g) were subjected to an intravital needle-injury model, as previously described.[38] Prior to vessel injury, a bolus of either 1 mg per kg hirudin or 0.5 mg per kg XChimera was systemically administered. Simultaneously, intravenous administration of DyLight 649-conjugated anti-GPIbβ antibody (X649 Emfret, Germany, 100 μg kg^{-1}) and Alexa 546-conjugated anti-fibrin antibody (0.5 mg kg^{-1}) was carried out to monitor thrombus formation and fibrin generation, respectively.

Following each injury, platelet thrombus formation and fibrin generation were monitored over a 15 min period using a confocal intravital microscopy platform (Nikon A1R-si; objective: Apo LWD, ×40 magnification, 1.15 numerical aperture, water immersion; sequential excitation: 488, 561, and 638 nm lasers; emission: 525/50, 595/50, and 700/75 nm filters; using NIS-Elements Advanced Research acquisition software). The microscope stage and objective were maintained at 37 °C throughout the experiment *via* a Peltier heater (OkoLab). Surface renders of confocal stacks representing thrombi from separate groups were generated using Imaris (Ver. 9.8 Bitplane AG, Zurich, Switzerland).

Quantitative analysis of thrombus volume over time: NIS-Elements software (Nikon, Japan) was used to apply a threshold to the DyLight 649-conjugated anti-mouse GP1bβ antibody signal for each *xyz* stack in a time series and was used to calculate the volume for each time point.

Quantitation of change in fibrin amount over time: the signal obtained from DyLight 649-conjugated anti-mouse GP1bβ antibody for each *xyz* stack in a time series was thresholded to create a mask. The total signal (AU) from the Alexa Fluor 546-conjugated anti-fibrin antibody within this mask (*i.e.*, the fibrin signal within the thrombus) for each time point was then quantified using NIS-Elements software (Nikon, Japan).

Statistical analysis: statistical significance between multiple treatment groups was analysed using an ordinary 2-way analysis of variance (ANOVA) with Tukey's multiple comparisons testing, with a single pooled variance (Prism 10.2, GraphPad Software, San Diego, CA). Data are presented as means ± SEM where '*n*' equals the number of independent experiments performed.

Author contributions

J. W. C. M. and R. J. P. conceived and designed the research project and designed the peptide and protein anticoagulants. J. W. C. M. and A. S. M. carried out the synthesis of the peptide and protein anticoagulants. J. R. R. and P. J. B. P. designed, performed and analysed experiments to determine inhibition constants against thrombin. J. R. R., J. A. S. and P. J. B. P. designed, performed and analysed crystallographic experiments. J. W. C. M., A. S. M., D. J. F., C. B. J. T., R. E. S., J. S. T. L., Z. Z., S. M. S., S. J. P., and R. J. P. designed, performed and analysed *in vitro* experiments. I. A., C. B. J. T. and R. E. S., performed and analysed *in vivo* experiments. J. W. C. M. and R. J. P. wrote the manuscript with the assistance of all authors.

Conflicts of interest

During the performance of all research studies I. A. and S. M. S. were employed by the Heart Research Institute, and affiliated with the University of Sydney, receiving salaries funded by academic grants. These authors are currently employed by ThromBio Pty Ltd, with the latter employment commencing after initial submission of the manuscript. S. P. J. is the founder and director of ThromBio Pty Ltd.

Data availability

The diffraction dataset for the structure reported in this article (doi: **https://doi.org/10.15785/SBGRID/1078**) was deposited with the SBGrid Data Bank (**https://data.sbgrid.org/**). Refined coordinates and structure factors were deposited at the Protein Data Bank with accession number 8RTN (**https://doi.org/10.2210/pdb8rtn/pdb**). The PDB validation report for 8RTN is provided with this manuscript as a SI file. Data is

available from the corresponding authors upon request. See DOI: https://doi.org/10.1039/d5sc04734j.

Acknowledgements

This work was funded through National Health and Medical Research Council of Australia Investigator Grants (APP1174941; to R. J. P.; APP1176016; to S. P. J.) and was also supported in part by national funds through FCT – Fundação para a Ciência e a Tecnologia, I. P. (Portugal) under project UIDB/04293/2020 and in the scope of research grants PTDC/BIA-BQM/2494/2020 (https://doi.org/10.54499/PTDC/BIA-BQM/2494/2020) and 2022.03363.PTDC (https://doi.org/10.54499/2022.03363.PTDC); and a New South Wales (NSW, Australia) Ministry of Health (MOH) Cardiovascular Senior Researcher Grants awarded to S. M. S. J. R.-R. acknowledges the support of grant RYC2021-033063-I funded by MCIN/AEI/10.13039/501100011033 and the European Union «NextGenerationEU»/PRTR. X-ray data collection was performed at BL13-XALOC beamline of ALBA Synchrotron with the collaboration of ALBA staff. The support of the X-Ray Crystallography, Biochemical and Biophysical Technologies and BioSciences Screening platforms of i3S (Porto, Portugal) is also acknowledged.

References

1 N. Townsend, *et al.*, *Nat. Rev. Cardiol.*, 2022, **19**, 133–143.
2 C. Magnussen, *et al.*, *N. Engl. J. Med.*, 2023, **389**, 1273–1285.
3 B. Vogel, *et al.*, *Lancet*, 2021, **397**, 2385–2438.
4 V. L. Feigin, *et al.*, *Lancet Neurol.*, 2021, **20**, 795–820.
5 B. C. V. Campbell, *et al.*, *Nat. Rev. Dis. Primers*, 2019, **5**, 70.
6 V. Saini, L. Guada and D. R. Yavagal, *Neurology*, 2021, **97**, S6–S16.
7 N. Mackman, W. Bergmeier, G. A. Stouffer and J. I. Weitz, *Nat. Rev. Drug Discovery*, 2020, **19**, 333–352.
8 J. S. Paikin, D. S. Wright and J. W. Eikelboom, *Blood Rev.*, 2011, **25**, 123–129.
9 B. Furie and B. C. Furie, *N. Engl. J. Med.*, 2008, **359**, 938–949.
10 S. J. Connolly, *et al.*, *Circulation*, 2008, **118**, 2029–2037.
11 M. Schenone, B. C. Furie and B. Furie, *Curr. Opin. Hematol.*, 2004, **11**, 272–277.
12 S. Gando, M. Levi and C.-H. Toh, *Nat. Rev. Dis. Primers*, 2016, **2**, 16037.
13 M. L. Kahn, *et al.*, *Nature*, 1998, **394**, 690–694.
14 J. Hauptmann, *Eur. J. Clin. Pharmacol.*, 2002, **57**, 751–758.
15 M. Di Nisio, S. Middeldorp and H. R. Büller, *N. Engl. J. Med.*, 2005, **353**, 1028–1040.
16 J. I. Weitz and N. C. Chan, *Blood*, 2020, **135**, 351–359.
17 K. A. Arsenault, J. Hirsh, R. P. Whitlock and J. W. Eikelboom, *Nat. Rev. Cardiol.*, 2012, **9**, 402–414.
18 J. W. C. Maxwell, P. M. E. Hawkins, E. E. Watson and R. J. Payne, *Acc. Chem. Res.*, 2023, **56**, 2688–2699.
19 M. A. Corral-Rodríguez, S. Macedo-Ribeiro, P. J. B. Pereira and P. Fuentes-Prior, *J. Med. Chem.*, 2010, **53**, 3847–3861.
20 A. Greinacher, N. Lubenow and P. Eichler, *Circulation*, 2003, **108**, 2062–2065.
21 T. J. Rydel, A. Tulinsky, W. Bode and R. Huber, *J. Mol. Biol.*, 1991, **221**, 583–601.
22 C. C. Liu, E. Brustad, W. Liu and P. G. Schultz, *J. Am. Chem. Soc.*, 2007, **129**, 10648–10649.
23 R. E. Thompson, *et al.*, *Nat. Chem.*, 2017, **9**, 909–917.
24 E. E. Watson, *et al.*, *ACS Cent. Sci.*, 2018, **4**, 468–476.
25 Y. S. Y. Hsieh, L. C. Wijeyewickrema, B. L. Wilkinson, R. N. Pike and R. J. Payne, *Angew. Chem., Int. Ed.*, 2014, **53**, 3947–3951.
26 B. M. Calisto, *et al.*, *Cell Chem. Biol.*, 2021, **28**, 26–33.
27 S. Lu, *et al.*, *J. Biol. Chem.*, 2021, **297**, 101322.
28 C. Y. Koh, *et al.*, *J. Biol. Chem.*, 2007, **282**, 29101–29113.
29 L. J. Dowman, *et al.*, *Chem. Commun.*, 2021, **57**, 10923–10926.
30 G. Soslau, *et al.*, *J. Biol. Chem.*, 2001, **276**, 21173–21183.
31 J. W. Williams and J. F. Morrison, *Methods Enzymol.*, 1979, **63**, 437–467.
32 B. C. Lechtenberg, S. M. V. Freund and J. A. Huntington, *J. Mol. Biol.*, 2014, **426**, 881–893.
33 S. Rahgozar, *et al.*, *Arthritis Rheum.*, 2007, **56**, 605–613.
34 R. S. Lovely, M. Moaddel and D. H. Farrell, *J. Thromb. Haemostasis*, 2003, **1**, 124–131.
35 N. S. Colwell, *et al.*, *Biochemistry*, 1998, **37**, 15057–15065.
36 K. Chen, *et al.*, *Biochemistry*, 2017, **56**, 3119–3128.
37 M. Dockerill, *et al.*, *Nat. Biotechnol.*, 2025, **43**, 186–193.
38 S. M. Agten, *et al.*, *Angew. Chem., Int. Ed.*, 2021, **60**, 5348–5356.
39 M. Cappello, *et al.*, *Am. J. Trop. Med. Hyg.*, 1996, **54**, 475–480.
40 A. C. Figueiredo, *et al.*, *Proc. Natl. Acad. Sci. U. S. A.*, 2012, **109**, E3649–E3658.
41 L. Wang, *et al.*, *Signal Transduction Targeted Ther.*, 2022, **7**, 48.
42 N. Boknäs, *et al.*, *Thromb. Haemostasis*, 2014, **112**, 558–565.
43 G. Soslau, S. J. Goldenberg, R. Class and B. Jameson, *Platelets*, 2004, **15**, 155–166.
44 G. W. Stone, *et al.*, *N. Engl. J. Med.*, 2008, **358**, 2218–2230.
45 E. E. Watson, *et al.*, *Proc. Natl. Acad. Sci. U. S. A.*, 2019, **116**, 13873–13878.
46 J. Juanhuix, *et al.*, *J. Synchrotron Radiat.*, 2014, **21**, 679–689.
47 W. Kabsch, *Acta Crystallogr., Sect. D: Biol. Crystallogr.*, 2010, **66**, 125–132.
48 M. D. Winn, *et al.*, *Acta Crystallogr., Sect. D: Biol. Crystallogr.*, 2011, **67**, 235–242.
49 P. A. Meyer, *et al.*, *Nat. Commun.*, 2016, **7**, 10882.
50 A. J. McCoy, *et al.*, *J. Appl. Crystallogr.*, 2007, **40**, 658–674.
51 A. C. Figueiredo, *et al.*, *PLoS One*, 2012, **7**, e34354.
52 P. Emsley, B. Lohkamp, W. G. Scott and K. Cowtan, *Acta Crystallogr., Sect. D: Biol. Crystallogr.*, 2010, **66**, 486–501.
53 D. Liebschner, *et al.*, *Acta Crystallogr., Sect. D: Biol. Crystallogr.*, 2019, **75**, 861–877.
54 A. Morin, *et al.*, *eLife*, 2013, **2**, e01456.
55 V. Ignjatovic, in *Methods in Molecular Biology*, Humana Press, New Jersey, 2013, vol. 992,pp. 111–120.
56 S. M. Schoenwaelder, *et al.*, *Blood*, 2009, **114**, 663–666.
57 S. P. Jackson, *et al.*, *J. Biol. Chem.*, 1994, **269**, 27093–27099.